Band-structure calculations of Fe1/3TaS2 and Mn1/3TaS2, and transport and magnetic properties of Fe0.28TaS2

Dijkstra, J.; Zijlema, P.J.; Haas, C.; Groot, R.A. de

Published in:
Journal of Physics%3A Condensed Matter

DOI:
10.1088/0953-8984/1/36/005

J. Phys.: Condens. Matter 1 (1989) 6363–6379. Printed in the UK

Band-structure calculations of $Fe_{1/3}TaS_2$ and $Mn_{1/3}TaS_2$, and transport and magnetic properties of $Fe_{0.28}TaS_2$

J Dijkstra†§, P J Zijlema†, C F van Bruggen†, C Haas† and R A de Groot‡

† Laboratory of Inorganic Chemistry, Materials Science Centre of the University, Nijenborgh 16, 9747 AG Groningen, The Netherlands

‡ Research Institute for Materials, Faculty of Science, Toernooiveld, 6525 ED Nijmegen, The Netherlands

Received 3 January 1989

Abstract. Band-structure calculations of ferromagnetic $Fe_{1/3}TaS_2$ and $Mn_{1/3}TaS_2$ using the augmented spherical-wave method are reported. The calculations give a spin magnetic moment of 4.35 μ_B per Fe for $Fe_{1/3}TaS_2$ and 4.18 μ_B per Mn for $Mn_{1/3}TaS_2$. The local moments at Fe and Mn induce a magnetic polarisation of the Ta $5d_{z^2}$ band, which is parallel to the local moment for $Fe_{1/3}TaS_2$ and antiparallel for $Mn_{1/3}TaS_2$. Measurements of the transport properties of $Fe_{0.28}TaS_2$ show a large spin-disorder contribution to the resistivity and a large anomalous Hall effect. The anomalous Hall effect is analysed in terms of side jump and skew scattering contributions. The large magnetisation anisotropy indicates the presence of Fe^{2+}, in agreement with the band-structure calculations.

1. Introduction

The transition-metal dichalcogenide layer compounds like TaS_2 easily allow the intercalation of a large variety of atoms and molecules in the van der Waals gap between the layers. The physical properties of these intercalation compounds have been studied extensively and several review papers have been published (Van den Berg-Voorhoeve 1976, Beal 1979, Friend and Yoffe 1987).

Compounds of interest for their magnetic properties are intercalates, in which 3d transition metals are used as intercalants. In the compounds T_xTaS_2 (T = V, Cr, Mn, Fe, Co, Ni; $x = 1/3, 1/4$) the transition-metal atoms form an ordered structure in the van der Waals gap between the TaS_2 layers. The physical properties of these compounds have been investigated in considerable detail by Parkin and Friend (1980a, b) and Parkin and Beal (1980). These investigations show that intercalation of V, Cr, Mn and Fe leads to ferromagnetic compounds, whereas Co and Ni intercalates are antiferromagnetic. From polarised neutron diffraction (Parkin *et al* 1983) the spatial magnetisation distribution of $Mn_{1/4}TaS_2$ was found to be mainly caused by local magnetic moments on the Mn atoms, but also a significant spin polarisation of the conduction electrons was measured.

§ Present address: Philips Research Laboratories, PO Box 80000, 5600 JA Eindhoven, The Netherlands.

0953-8984/89/366363 + 17 $02.50

$Fe_{1/3}TaS_2$ is the only ferromagnetic intercalate of TaS_2 that has an easy axis of magnetisation perpendicular to the layers, i.e. along the crystallographic *c* axis (Eibschütz *et al* 1975, 1981, Parkin and Friend 1980a), which makes it an interesting material for studies of the polar magneto-optical Kerr effect (Wijngaard *et al* 1988) and the anomalous Hall effect (Parkin and Friend 1980b). $Mn_{1/3}TaS_2$ is also ferromagnetic, but its easy axis of magnetisation is perpendicular to the *c* axis.

All 3d transition-metal intercalates of TaS_2 show metallic conductivity. The temperature dependence of the electrical resistivity indicates a strong interaction of the conduction electrons with the local magnetic moments, which leads to a strong spin-disorder scattering.

Little is known about the band structure of the 3d transition-metal intercalates of TaS_2: no band-structure calculations have been reported so far. However, some spectroscopic information about the electronic structure does exist. Reflectivity data indicate a broadening of the S 3p valence band and the Ta $5d_{z^2}$ conduction band, as compared with 2H-TaS_2 (Parkin and Beal 1980). Angle-resolved photo-emission shows that in the 3d intercalates the energy gap between the Ta $5d_{z^2}$ band and the S 3p band has increased relative to 2H-TaS_2 (Barry and Hughes 1983a). These changes are attributed to the transfer of electrons from the transition-metal atoms to the Ta $5d_{z^2}$ conduction band. According to x-ray photo-electron spectroscopic (XPS) data the Fe and Mn atoms in the intercalation compounds are present as divalent ions (Barry and Hughes 1982, 1983b).

Because no band-structure calculations of transition-metal intercalates were available, the experimental results were usually discussed in terms of the so-called rigid-band model. In this model it is assumed that the electronic energy bands in the host lattice remain unchanged in the intercalation compounds, and that only the Fermi level changes as a result of electron transfer from the intercalated atoms to the host lattice. However, the experimental data clearly show that the rigid-band model can only serve as a first-order approximation, and that important deviations from this model must be present.

In this paper we present band-structure calculations of the ferromagnetic intercalation compounds $Fe_{1/3}TaS_2$ and of $Mn_{1/3}TaS_2$. The deviations from the rigid-band model are discussed. We also report measurements of the magnetic and transport properties of $Fe_{0.28}TaS_2$ and discuss the results in terms of the calculated band structure. Extensive measurements of the anomalous Hall effect are reported, and analysed in terms of skew scattering and side jump contributions.

2. Crystal structure

The crystal structure of $M_{1/3}TaS_2$ (M = Mn, Fe), shown in figure 1, can be described in space group $P6_322$ (D_6^6, No 182 in the *International Tables*), with atoms on the following special positions:

2 Fe/Mn	in (2c)	$(\frac{1}{3}, \frac{2}{3}, \frac{1}{4}), (\frac{2}{3}, \frac{1}{3}, \frac{3}{4})$
2 Ta_1	in (2a)	$(0, 0, 0), (0, 0, \frac{1}{2})$
4 Ta_2	in (4f)	$(\frac{1}{3}, \frac{2}{3}, z), (\frac{2}{3}, \frac{1}{3}, z), (\frac{1}{3}, \frac{2}{3}, \frac{1}{2} + z), (\frac{2}{3}, \frac{1}{3}, \frac{1}{2} + z)$ with $z \simeq 0$
12 S	in (12i)	(x, y, z) etc. with $x \simeq \frac{1}{3}, y \simeq 0, z \simeq \frac{1}{8}$.

The structure consists of S–Ta–S sandwiches in which Ta has a trigonal-prismatic

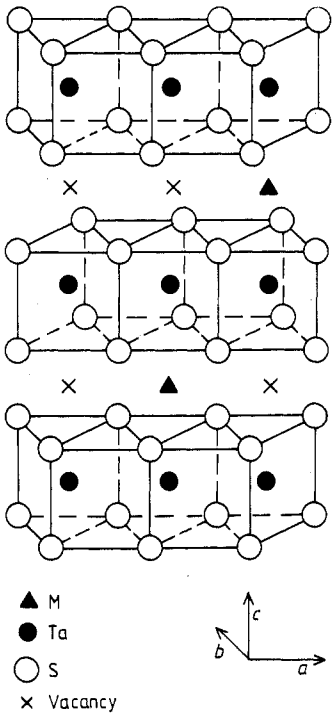

Figure 1. The crystal structure of $Fe_{1/3}TaS_2$.

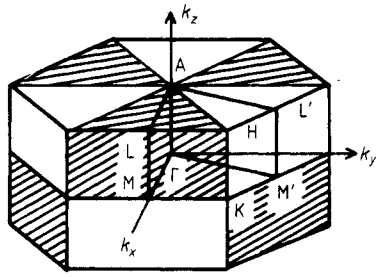

Figure 2. The hexagonal Brillouin zone with the high-symmetry points.

Table 1. Input parameters (Å) for the ASW band-structure calculations. Lattice constants a, c and z_S (Van Laar *et al* 1970, Parkin and Friend 1980a). $a_0 = a/\sqrt{3}$ for the intercalates. d(Ta–S) is the Ta–S distance. The distance along the c axis between S layers within one sandwich is $d(S\text{–}S)_{intra}$ and between neighbouring sandwiches $d(S\text{–}S)_{inter}$. r_i are the Wigner–Seitz sphere radii. Data for 2H-TaS_2 are given for comparison (Dijkstra *et al* 1989).

	2H-TaS_2	$Mn_{1/3}TaS_2$	$Fe_{1/3}TaS_2$
a	3.316	5.748	5.737
c	12.070	12.635	12.284
z_S	0.125	0.125	0.130
a_0	3.316	3.319	3.312
d(Ta–S)	2.44	2.48	2.49
$d(S\text{–}S)_{intra}$	3.02	3.16	3.19
$d(S\text{–}S)_{inter}$	3.02	3.16	2.95
r_{Ta}	1.373	1.193	1.137
r_S	1.772	1.765	1.765
$r_{Fe/Mn}$	—	1.193	1.137
$r_{emptysphere}$	—	1.193	1.137

coordination by S. The stacking of the TaS_2 slabs is the same as in 2H-TaS_2. The parameters used in the band-structure calculations for 2H-TaS_2, $Mn_{1/3}TaS_2$ and $Fe_{1/3}TaS_2$ are given in table 1. The length of the a axis is nearly the same in the three compounds. The TaS_2 sandwiches are only slightly altered by intercalation: the

Ta–S distance increases from 2.44 to 2.49 Å and the TaS_2 sandwich thickness from 3.02 to 3.19 Å. The c/a ratio of the octahedron of six S surrounding the 3d ion is 1.780/2 for Fe and 1.904/2 for Mn. Thus there is an appreciable trigonal elongation of the (Fe,Mn)–6S octahedron; the value of c/a for an undistorted octahedron is 1.633/2. In the structure of $Fe_{1/3}TaS_2$ and $Mn_{1/3}TaS_2$ there are two types of Ta atoms: Ta_1 atoms have no direct Fe(Mn) neighbours, whereas each Ta_2 has one Fe(Mn) neighbour. The Fe(Mn) atoms are linearly coordinated by two Ta_2 atoms.

3. Band-structure calculations

Band-structure calculations were performed for $Mn_{1/3}TaS_2$ and $Fe_{1/3}TaS_2$ using the augmented spherical wave (ASW) method of Williams *et al* (1979). Exchange and correlation are treated in the local-density approximation (Hedin and Lundquist 1971). Scalar relativistic effects were included (Methfessel and Kübler 1982). In the ASW method the crystal is divided into so-called Wigner–Seitz spheres around each atom. The sum of the volumes of these spheres is equal to the unit-cell volume. Empty spheres were included in the calculations of the intercalates at the empty (2b) and (2d) sites in the intercalant layers. Within the Wigner–Seitz spheres the potential is taken to be spherically symmetric. The basis functions were composed of 6s, 6p and 5d on Ta; 4s, 4p and 3d on Mn and Fe; 3s and 3p on S; and 1s and 2p on the empty spheres. The Ta 5f, Mn/Fe 4f, S 3d and Ze 3d functions were included in the internal summation of the three-centre contributions to the matrix elements, which can be regarded as treating them as a perturbation. The calculations are self-consistent. The input and output charge within each Wigner–Seitz sphere differed by less than 10^{-5} electron in the last iteration.

The hexagonal Brillouin zone is given in figure 2, in which the high-symmetry points are indicated. The crystal-structure parameters and Wigner–Seitz sphere radii used in the band-structure calculations are given in table 1.

In order to investigate deviations from the rigid-band model it is necessary to calculate the electronic structure of the host compound 2H-TaS_2 with the same method. Our results for the band structure and density of states of 2H-TaS_2 were reported previously (Dijkstra *et al* 1989). These results are in agreement with the ASA-LMTO calculations by Guo and Liang (1987).

3.1. $Mn_{1/3}TaS_2$

The calculated spin-up ($\uparrow$) and spin-down ($\downarrow$) density of states (DOS) of $Mn_{1/3}TaS_2$ in the fully ordered ferromagnetic state at $T = 0$ K is plotted in figure 3(*a*). The total DOS is the sum of the contributions of the majority ($\uparrow$) and minority ($\downarrow$) electrons. In figures 3(*b*)–(*e*) the partial DOS, i.e. the contributions of the different atoms to the total DOS, are shown. The Mn partial DOS consists almost exclusively of 3d states, and the Ta DOS consists of 5d states. The band around −15 eV is mainly composed of S 3s states. The bands at higher energy are predominantly of S 3p character with some S 3d character mixed in. The dispersion of the eigenvalues along high-symmetry directions in the Brillouin zone is shown in figure 4.

The bands that are localised mainly on the host TaS_2 show strong resemblance with the bands of 2H-TaS_2 (see Dijkstra *et al* 1989). The Ta 5d states are split into a Ta $5d_{z^2}$ band and Ta 5d bands at higher energy, due to the trigonal-prismatic coordination of Ta by S. The Ta $5d_{z^2}$ band, which is half-filled with one electron per Ta in 2H-TaS_2, is filled

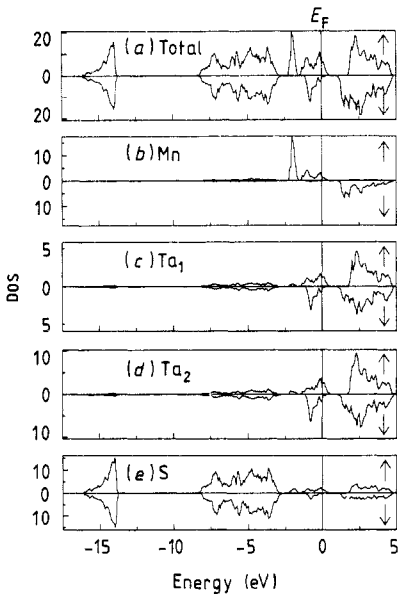

Figure 3. (*a*) Total density of states (DOS) of ferromagnetic $Mn_{1/3}TaS_2$. (*b*) Partial Mn DOS. (*c*) Partial Ta_1 DOS. (*d*) Partial Ta_2 DOS. (*e*) Partial S DOS. Units: states eV^{-1} (unit cell)$^{-1}$.

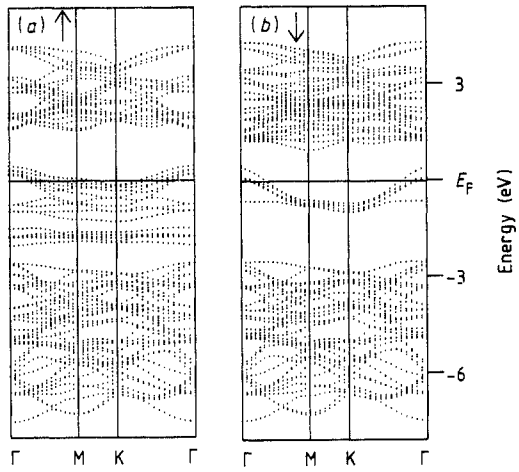

Figure 4. The electron energy bands of ferromagnetic $Mn_{1/3}TaS_2$.

in $Mn_{1/3}TaS_2$ for about 85%. This is due to electron transfer from the Mn atom to the Ta $5d_{z^2}$ band. The mixing of S 3p states with Ta 5d is stronger than the mixing of S 3p with Mn 3d, because the radial extension of Ta 5d states is larger than that of Mn 3d states. The S 3s and S 3p bands show very little magnetic polarisation.

The Mn 3d states are situated in the same energy region as the Ta 5d states (see figure 3). The Mn 3d ↑ states show the crystal-field splitting of the (distorted) octahedron of S surrounding Mn, with a lower t_{2g} and a higher e_g band. The e_g ↑ states hybridise with the Ta $5d_{z^2}$ ↑ states, causing a larger e_g ↑ than t_{2g} ↑ band width. The Mn 3d ↑ states show less hybridisation than the 3d ↓ states. The Mn t_{2g} ↑ band is only 0.6 eV wide. The Mn–Mn distances are too large (5.748 Å) for significant Mn–Mn overlap.

The large intra-atomic exchange splitting of 3.5 eV between Mn 3d ↑ and Mn 3d ↓ leads to a magnetic moment of $+4.4\ \mu_B$ within the Mn Wigner–Seitz sphere ($4.6\ \mu_B$ ↑ and $0.2\ \mu_B$ ↓). There is a small magnetic moment of $+0.03\ \mu_B$ at the S atoms, as a consequence of hybridisation. The Mn magnetic moments also induce through covalency some magnetisation density at the Ta atoms. Since the Mn 3d ↑ states lie mainly below the Ta $5d_{z^2}$ band, hybridisation with these Mn 3d ↑ states shifts the Ta $5d_{z^2}$ ↑ band to higher energy. Hybridisation with Mn 3d ↓ shifts the $5d_{z^2}$ ↓ band to lower energy, because the Mn 3d ↓ states lie well above the Ta $5d_{z^2}$ band. As a consequence, the net magnetic polarisation of the Ta $5d_{z^2}$ band is opposite to that of Mn. Within the Wigner–Seitz spheres of Ta atoms neighbouring Mn—i.e. type Ta_2 atoms—we find a magnetic polarisation of $-0.15\ \mu_B$ and on Ta_1 of $-0.10\ \mu_B$. The resulting calculated total magnetic moment per Mn ($MnTa_3S_6$) is $4.18\ \mu_B$. The value is much lower than the value of $5\ \mu_B$ for Mn^{2+} (d^5), which is expected in a simple rigid-band model. However, the calculated value is in agreement with experimental data. From saturation-magnetisation measurements a value of $3.9\ \mu_B$ is obtained (Hulliger and Pobitschka 1970). Susceptibility data

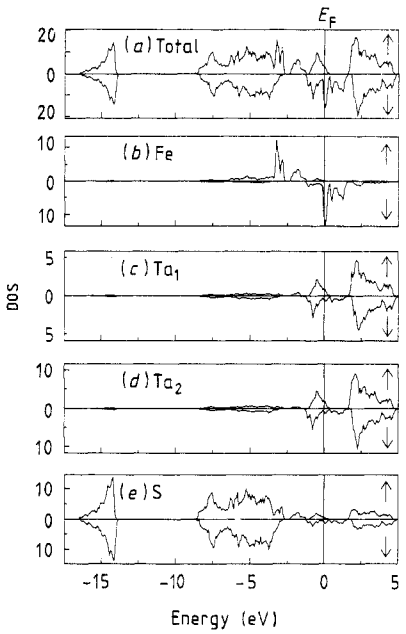

Figure 5. (*a*) Total density of states (DOS) of ferromagnetic $Fe_{1/3}TaS_2$. (*b*) Partial Fe DOS. (*c*) Partial Ta_1 DOS. (*d*) Partial Ta_2 DOS. (*e*) Partial S DOS. Units: states eV^{-1} (unit cell)$^{-1}$.

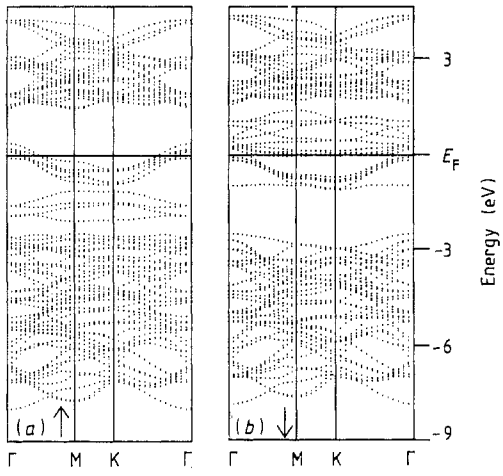

Figure 6. The electron energy bands of ferromagnetic $Fe_{1/3}TaS_2$.

give values for μ_{eff} of 4.67 μ_B (Hulliger and Pobitschka 1970), 4.82 μ_B (Van den Berg and Cossee 1968) and 5.97 μ_B (Parkin and Friend 1980a), which should be compared with the value of $\mu_{eff} = 5.92\ \mu_B$ for Mn^{2+} (d^5). Van Laar *et al* (1970) find with neutron diffraction a moment of 4.0 μ_B on Mn in the comparable compound $Mn_{1/3}NbS_2$. Polarised neutron diffraction on $Mn_{1/4}TaS_2$ showed a magnetic moment of 4.2 μ_B on Mn and in addition a significant spin polarisation of the conduction electrons on the Ta atoms (Parkin *et al* 1983).

3.2. $Fe_{1/3}TaS_2$

The calculated total DOS and the energy bands of $Fe_{1/3}TaS_2$ are given in figures 5(*a*) and 6. In figures 5(*b*)–(*e*) the contributions of the different atoms to the total DOS are plotted. The partial Ta and S DOS of $Fe_{1/3}TaS_2$ are similar to those of $Mn_{1/3}TaS_2$ (figures 3(*c*)–(*e*)): filled S 3s and 3p bands and a Ta $5d_{z^2}$ band at the Fermi level, split off from the other Ta 5d states. Electrons are transferred from Fe to the Ta $5d_{z^2}$ band, and as a result the Ta $5d_{z^2}$ band is more than half, but not completely, filled. The Fe 3d ↑ states lie well below E_F and are completely filled. The Fe 3d ↓ states are at the top of the Ta $5d_{z^2}$ band and have a large density of states at E_F. Because of the complete occupation of the Fe 3d ↑ and the partial occupation of the Fe 3d ↓ states, Fe has a valency less than 3. There are 4.75 spin-up and 1.15 spin-down electrons inside the Fe Wigner–Seitz sphere and the calculated local spin magnetic moment on Fe is 3.6 μ_B. In this compound there is also a magnetic polarisation of the host lattice amounting to 0.75 μ_B per Fe: +0.10 μ_B on each Ta and +0.075 μ_B on each S. The positive polarisation of the Ta $5d_{z^2}$ band is

mainly a consequence of the Fe–Ta covalency of the spin-down states. Contrary to $Mn_{1/3}TaS_2$, the magnetic polarisation of the host lattice in $Fe_{1/3}TaS_2$ is in the same direction as the moments of the intercalant atoms. The total spin magnetic moment per Fe ($FeTa_3S_6$) amounts to 4.35 μ_B.

Band-structure calculations of the intercalation compound $Fe_{1/3}TiS_2$ show a small negative polarisation of the Ti atoms and a small positive polarisation of the S atoms (Suzuki *et al* 1987). The calculated moment per Fe in $Fe_{1/3}TiS_2$ is 2.45 μ_B, much smaller than the value found for $Fe_{1/3}TaS_2$.

3.3. Discussion

The calculated electronic structure of $Mn_{1/3}TaS_2$ and $Fe_{1/3}TaS_2$ can be understood by using the rigid-band model as a starting point. The TaS_2 partial DOS indeed shows a strong resemblance to that of 2H-TaS_2 and electron transfer of Mn and Fe to the host leads to an increased filling of the Ta $5d_{z^2}$ band. However, the self-consistent band-structure calculations give much more information, such as the positions of the intercalant states, the mixing of these states with host bands and the changes in the host band structure itself. In this section these effects, which go beyond the rigid-band model, are discussed.

First of all the calculation gives the positions of the exchange-split Mn and Fe 3d states. The Fe 3d states lie at lower energy than the Mn states as a consequence of the higher atomic number of Fe. The intra-atomic exchange splitting (ΔE_{ex}) is related to the local magnetic moment on the 3d ion (Mn, ΔE_{ex} = 3.5 eV, μ_{Mn} = 4.4 μ_B; Fe, ΔE_{ex} = 3.2 eV, μ_{Fe} = 3.6 μ_B).

The intercalant 3d states hybridise strongly with host states: Mn 3d ↑ (e_g) mainly with Ta $5d_{z^2}$ ↑, Mn 3d ↓ with Ta 5d ↓, Fe 3d ↑ with S 3p ↑, and Fe 3d ↓ with Ta $5d_{z^2}$ ↓. The amount of hybridisation is chiefly determined by the relative energy of the states involved.

The Mn—Ta interaction causes a negative magnetic polarisation of the Ta $5d_{z^2}$ band in $Mn_{1/3}TaS_2$. In $Fe_{1/3}TaS_2$ the Ta $5d_{z^2}$ bands are shifted in the same direction as in $Mn_{1/3}TaS_2$ (the $5d_{z^2}$ ↑ to higher and the $5d_{z^2}$ ↓ to lower energy), but due to the large Fe t_{2g} ↓ /Ta $5d_{z^2}$ ↓ hybridisation some Ta DOS is shifted to energies above E_F. Together with the increased filling of the Ta $5d_{z^2}$ band, this results in a net positive polarisation of the Ta atoms, i.e. a polarisation in the same direction as the Fe moments.

The most striking difference in the TaS_2 part of the electronic structure is the increase of the Ta 5d/S 3p gap as compared to the host compound. For 2H-TaS_2 the calculated indirect d/p gap (Dijkstra *et al* 1989, Guo and Liang 1987) is about zero, while the direct gap at Γ is 0.82 eV. In the calculation of 2H-TaS_2 the S 3d functions were included explicitly as basis functions. In the calculations of the 3d intercalates the S 3d functions were included only in the three-centre contributions to the matrix elements, but were not included in the secular matrix. To test the influence of the omission of the S 3d functions we have also calculated the band structure of 2H-TaS_2 without S 3d as basis functions. The result is similar to the band-structure calculation with the S 3d states included in the basis set: the S 3s, 3p and Ta $5d_{z^2}$ band widths are the same, only the unfilled Ta 5d band is a little wider. However, the d/p gap is about 0.5 eV larger: the indirect gap becomes 0.53 eV and the direct gap 1.33 eV (compared to about 0 eV and 0.82 eV, respectively, when S 3d is included in the secular matrix).

In $Fe_{1/3}TaS_2$ the indirect Ta 5d/S 3p gap in the spin-down direction is 1.5 eV and in $Mn_{1/3}TaS_2$ it is 1.6 eV, while the values for the direct gaps in Γ are 1.66 and 2.12 eV,

Table 2. The band width W of the S 3p band and the length of the c axis.

	2H-TaS_2	$Fe_{1/3}TaS_2$	$Mn_{1/3}TaS_2$
c axis (Å)	12.070	12.284	12.635
W (S 3p) (eV)	6.17	5.92	5.58

respectively. The calculated increase in the Ta 5d/S 3p gap by intercalation is thus about 1 eV. Two reasons can be given. First, the addition of extra electrons on Ta makes Ta more electropositive and thereby increases the Ta–S ionicity. Secondly, the S 3p and Ta $5d_{z^2}$ bands become narrower (see below) and generally a narrowing of the bands will lead to an increase of the gap.

The direct and indirect d/p gaps in $Fe_{1/3}TaS_2$ measured by angle-resolved photoelectron spectroscopy are 1.5 and 1.1 eV (Barry and Hughes 1983a), in reasonable agreement with our calculation.

The width of the S 3p band is mainly determined by the S–S inter-sandwich and intra-sandwich interactions along the c direction, since the lowest and the topmost states of this set of bands are of S $3p_z$ origin. The data in table 2 illustrate that an increase in c axis is accompanied by a narrowing of the S 3p band.

$Fe_{1/3}TaS_2$ and $Mn_{1/3}TaS_2$ are both metallic, since the Ta $5d_{z^2}$ band is partly filled. The density of states at the Fermi level $N(E_F)$ can be decomposed into contributions of the intercalant and the host states. The intercalant 3d electrons are rather localised—their band width is small—and they probably play no role of importance as charge carriers in the electrical transport properties. The host contribution to $N(E_F)$ (in states per electronvolt per unit TaS_2) is, for spin-up and spin-down respectively: 0.91 and 0.37 for $Mn_{1/3}TaS_2$ and 0.61 and 0.35 for $Fe_{1/3}TaS_2$. In 2H-TaS_2 $N(E_F) = 4.01$ states per electronvolt per unit TaS_2.

Inspection of the calculated Ta $5d_{z^2}$ bands of the two intercalation compounds around E_F shows the presence of empty states (holes) around Γ in the Ta $5d_{z^2}$ band for both spin directions: in $Mn_{1/3}TaS_2$ 0.04 $\downarrow$ holes and 0.26 $\uparrow$ holes and in $Fe_{1/3}TaS_2$ 0.04 $\downarrow$ holes and 0.10 $\uparrow$ holes per Ta atom.

Taking the number of holes in the Ta $5d_{z^2}$ band as a starting point, we can give a description of the calculated electronic structure, which is easy to compare with the rigid-band model. The numbers given in the analysis below are slightly different from the electron-occupation numbers within the Wigner–Seitz spheres. The reason is that the electron charges within Wigner–Seitz spheres strongly reflect covalency, while in the following description we adopt a completely ionic point of view, i.e. every band is assigned to one type of atom. For instance, we assign the $5d_{z^2}$ band to Ta only. According to this description S is present as S^{2-}, since the S 3s and 3p bands are completely filled.

In $Mn_{1/3}TaS_2$ the total number of holes in the Ta $5d_{z^2}$ band is $0.26 + 0.04 = 0.30$ per formula unit. This number corresponds to $Mn^{2.10+}$, i.e. $3d^{4.90}$, close to the value of divalent Mn. The magnetic polarisation of the $5d_{z^2}$ band is $-0.26 + 0.04 = -0.22\ \mu_B$ per Ta, and the total magnetic moment per Mn is now $4.90 - 3 \times 0.22 = 4.24\ \mu_B$. The analysis in § 3.1 resulted in $4.18\ \mu_B$.

In $Fe_{1/3}TaS_2$ there are $0.10 + 0.04 = 0.14$ holes per formula unit in the Ta $5d_{z^2}$ band. Consequently Fe is present as $Fe^{2.58+}$, i.e. $3d^{5.42}$. The spin magnetic moment on Fe is $5 - 0.42 = 4.58\ \mu_B$. The polarisation of the $5d_{z^2}$ band of $-0.10 + 0.04 = -0.06\ \mu_B$ per

formula unit results in a moment of $4.58 - 0.18 = 4.40\ \mu_B$ per Fe, in agreement with the value of $4.35\ \mu_B$ calculated in § 3.2.

An important difference between the Mn and the Fe intercalate is increased filling of the Ta d_{z^2} band in $Fe_{1/3}TaS_2$, as compared to $Mn_{1/3}TaS_2$. In $Fe_{1/3}TaS_2$ only 0.14 holes per Ta are left in the d_{z^2} band, while in $Mn_{1/3}TaS_2$ there are 0.30 holes. This shows Mn to be divalent, while the mean valency of Fe is about 2.6+. Direct experimental support of the Fe valency comes from the isomer shift in Mössbauer spectra. Eibschütz *et al* (1975, 1981) measured an isomer shift of 0.83 mm s^{-1} with respect to iron metal, which is slightly larger than the shift for FeS (0.77 mm s^{-1}) and other sulphides with Fe in an octahedral environment, indicating a more ionic Fe–S bond in $Fe_{1/3}TaS_2$ than in FeS. The valency of Fe is thus somewhat higher than Fe^{2+} in FeS.

4. Experimental results for $Fe_{0.28}TaS_2$

Polycrystalline powder of $Fe_{1/3}TaS_2$ is synthesised by heating together proper amounts of the elements at 850 °C for 10 days and, after repowdering, heating again for another 10 days. Single crystals were grown by iodine vapour transport for 15 days in a temperature gradient from 950 to 800 °C; the crystals grow at the colder end of the tube. Crystal platelets with surfaces up to 2 cm^2 and 0.1 cm thick are obtained. X-ray diffraction showed clearly the $\sqrt{3} \times \sqrt{3}$ superstructure reflections. The cell parameters at room temperature are $a = 5.763$ Å and $c = 12.277$ Å.

All measurements reported in this section are performed on single-crystalline platelets from one batch of Fe_xTaS_2 with composition $x = 0.28$, as deduced from chemical analysis.

4.1. Magnetic properties

Magnetic measurements were performed using a Foner magnetometer in the temperature range below the Curie temperature T_C and a Faraday balance at higher temperatures.

Magnetisation isotherms of $Fe_{0.28}TaS_2$ as a function of applied magnetic field H_A were measured in the temperature region from 4.2 to 90 K. The magnetic field was applied in the direction normal to the layers, i.e. along the easy axis of magnetisation. The maximum applied field was 5 T.

The spontaneous magnetisation M_S is obtained by extrapolating the high-field part of the measured magnetisation isotherm to the applied field value $\mu_0 H_A = \mu_0 N_D M$, corresponding to an internal field $\mu_0 H_i = \mu_0(H_A - N_D M) = 0$. The permeability of the vacuum is μ_0. The demagnetising field is $-N_D M$ where N_D is the demagnetising factor, which is 1 in the case of a thin plate.

The spontaneous magnetisation M_S of $Fe_{0.28}TaS_2$ as a function of temperature is given in figure 7. The Curie temperature, obtained by extrapolating M_S to zero, is 70 K. The value of M_S is 1.67×10^5 A m^{-1} ($\mu_0 M_S = 0.21$ T) at 4.2 K, corresponding to a saturation moment of $3.86\ \mu_B$ per Fe atom.

In a local moment ferromagnet the presence of collective spin excitations normally gives rise to a Bloch $T^{3/2}$ law for the temperature dependence of $\Delta M_S(T) \times M_S(T = 0) - M_S(T)$. However, in our data for $Fe_{0.28}TaS_2$ the spontaneous magnetisation shows a quadratic dependence of ΔM_S on temperature up to 50 K (figure 8). Such a T^2 dependence of ΔM_s is also observed for ferromagnetic $Cr_{1/3}TaS_2$ (Parkin and Friend

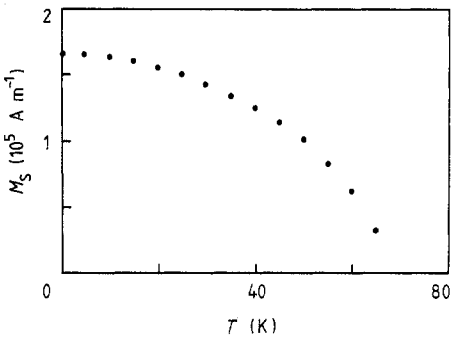

Figure 7. Spontaneous magnetisation M_S of $Fe_{0.28}TaS_2$ parallel to the c axis as a function of temperature T.

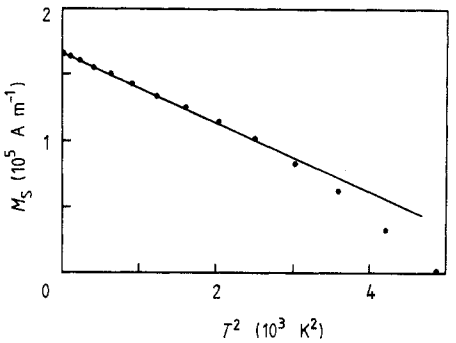

Figure 8. Spontaneous magnetisation M_S of $Fe_{0.28}TaS_2$ parallel to the c axis as a function of T^2.

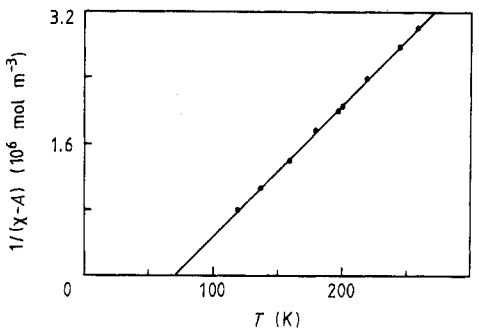

Figure 9. Inverse magnetic susceptibility of $Fe_{0.28}TaS_2$ as a function of temperature. The straight line corresponds to the least-squares Curie–Weiss fit.

1980a). The exponent $n = 2$ is predicted by spin-wave theory for a two-dimensional ferromagnet (Coqblin 1977). Therefore the observed temperature dependence of the low-temperature magnetisation of $Fe_{1/3}TaS_2$ shows that in this compound the magnetic interactions are much stronger within the layers than between Fe atoms in different layers.

At low temperatures a large magnetic field is required to reverse the spins (see figure 11). The coercive field is about 5 T at 4.2 K; it decreases strongly with increasing temperature and is very small above 40 K.

The magnetic susceptibility χ of $Fe_{0.28}TaS_2$ was measured above T_C with an applied magnetic field $\mu_0 H_A$ of 0.8 T parallel to the c axis. The results were corrected for the diamagnetic contributions of the core electrons. The measured susceptibility was fitted to a Curie–Weiss law of the form

$$\chi = A + C/(T - \theta_p). \tag{1}$$

A is a temperature-independent term due to the conduction electrons (Pauli paramagnetism) and/or transition-metal ions (van Vleck paramagnetism). The temperature is T and the paramagnetic Curie temperature θ_p. The Curie constant is $C = N\mu_{eff}^2/3k_B$, where N is the number of magnetic moments per unit volume, μ_{eff} is the effective magnetic moment and k_B is the Boltzmann constant. A least-squares fit of $(\chi - A)^{-1}$ versus T gives $A = 6.4 \times 10^{-9}$ m^3 mol^{-1}, $\mu_{eff} = 3.85\,\mu_B$ and $\theta_p = 71$ K (see figure 9).

Our magnetic data are in reasonable agreement with data reported by Eibschütz *et al* (1975, 1981) for samples of $Fe_{0.28}TaS_2$. These authors report a value of $M_S = 3.5\ \mu_B$ per Fe at $T = 0$ K. By fitting susceptibility data for $H \parallel c$ to a Curie–Weiss law without a temperature-independent term, values of $\mu_{eff} = 4.37\ \mu_B$ (Eibschütz *et al* 1975) and $\mu_{eff} = 4.50\ \mu_B$ (Eibschütz *et al* 1981) were obtained. If we analyse our susceptibility data in this way (i.e. $A = 0$) we obtain a value of $\mu_{eff} \simeq 4.33\ \mu_B$, but χ^{-1} versus T is not a straight line.

The magnetic properties of Fe_xTaS_2 depend strongly on the composition x (Eibschütz *et al* 1981). Parkin and Friend (1980a) report rather different values of the magnetic properties ($T_C = 40$ K), probably due to the different composition of their sample ($x = 0.33$, according to x-ray fluorescence).

The difference between the observed magnetic moments and the moment obtained from our band-structure calculation can be partly due to orbital contributions. In the ASW calculation spin–orbit interaction is not taken into account, so that the calculated moments are spin-only moments. Orbital contributions are expected to be large for Fe^{2+} ions (and small for Mn^{2+}), as follows from crystal-field considerations. Other indications of large orbital contributions are the strong anisotropy of the magnetic susceptibility, and the associated anisotropic g-factor (Parkin and Friend 1980a).

The remarkable difference between the magnetic anisotropy of $Fe_{1/3}TaS_2$ (easy axis $\parallel c$) and $Mn_{1/3}TaS_2$ (easy axis $\perp c$) is also a result of orbital contributions. The two main interactions responsible for the magnetic anisotropy are the single-ion anisotropy and the dipolar interactions. In a strongly two-dimensional array of magnetic moments the dipolar interactions lead to a preferred direction of magnetisation parallel to the layers. The large magnetic anisotropy of $Fe_{1/3}TaS_2$ is a single-ion effect due to interaction of the spin with the orbital moment of the partially occupied Fe 3d $\downarrow$ band (Parkin and Friend 1980a). As a result of the trigonal distortion of the octahedra of S atoms, the 3d t_{2g} states are split into a_{1g} and e_g^a states. According to our band-structure calculations the e_g^a states (derived from t_{2g}) have the lower energy. This was also deduced by Parkin and Friend (1980a) from crystal-field theory. These e_g^a states have an orbital momentum parallel to the c axis, and spin–orbit interaction leads to a preferred orientation of the spin parallel to the c axis. In $Fe_{1/3}TaS_2$ the single-ion anisotropy is larger than the dipolar interactions, leading to an easy axis of magnetisation parallel to the c axis. In $Mn_{1/3}TaS_2$ the Mn 3d $\downarrow$ band is unoccupied, while the Mn 3d $\uparrow$ band is nearly completely occupied. The remaining holes in the 3d $\uparrow$ band occupy e_g^b-type states, which have no orbital momentum (in first order). Therefore the magnetic anisotropy of $Mn_{1/3}TaS_2$ is dominated by dipolar interactions, leading to an easy axis normal to c.

4.2. Electrical resistivity

The electrical resistivity of ferromagnetic metals is composed of three contributions. At $T = 0$ K there is only the temperature-independent residual resistivity ρ_{res}, due to crystallographic disorder, crystal defects or the presence of foreign atoms. At higher temperatures also spin-disorder scattering and electron–phonon scattering contribute to the resistivity. The spin-disorder scattering increases with temperature up to the Curie temperature T_C. Above T_C this spin-disorder contribution ρ_{sd} remains approximately constant, since the spin disorder is then nearly complete. The resistivity increase above T_C is mainly due to electron–phonon interactions. Except at very low temperatures, the phonon contribution to the resistivity ρ_{ph} is proportional to T, according to the Bloch–Grüneisen law.

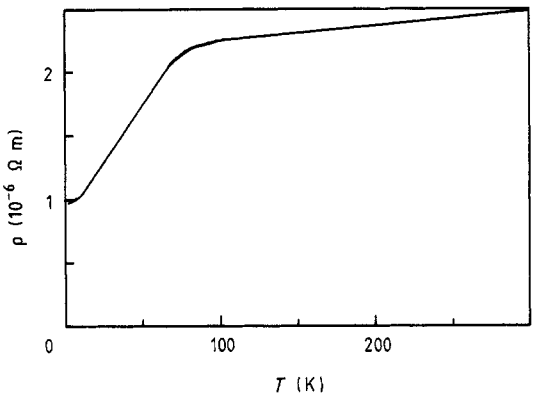

Figure 10. The temperature dependence of the specific resistivity of $Fe_{0.28}TaS_2$, measured parallel to the layers.

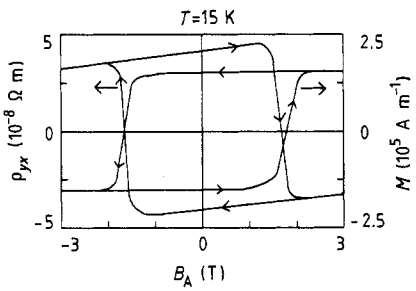

Figure 11. The magnetisation M and the Hall resistivity ρ_{yx} of $Fe_{0.28}TaS_2$ at 15 K as a function of the applied magnetic field.

The electrical resistivity (figure 10) of a single-crystalline platelet $Fe_{0.28}TaS_2$ was measured with the current parallel to the layers, i.e. normal to the c axis. The residual resistivity, $1.0 \times 10^{-6}\ \Omega$ m, is fairly high, presumably due to Fe deficiency and incomplete ordering of the Fe atoms. The maximum spin-disorder contribution is $1.2 \times 10^{-6}\ \Omega$ m, indicating a strong interaction between the Ta d_{z^2} conduction electrons and the intercalant magnetic moments. The slope $\partial\rho/\partial T$ shows a sharp change in magnitude at 75 K. The Curie temperature determined in this way is in reasonable agreement with the value of 70 K obtained from magnetic measurements. From the slope of the resistivity versus temperature above T_C the phonon contribution to ρ can be deduced: $\partial\rho_{ph}/\partial T = 1.0 \times 10^{-9}\ \Omega\ \text{m K}^{-1}$.

Our results are in agreement with data reported by Eibschütz *et al* (1981). Parkin and Friend (1980b) find about the same spin-disorder contribution, but a smaller residual resistivity in a more stoichiometric crystal.

4.3. Anomalous and normal Hall effect

Measurements show that the Hall effect of $Fe_{0.28}TaS_2$ is not a linear function of the applied magnetic field H_A at temperatures below T_C. It is found that the shape of the ρ_{yx} versus H_A isotherms of $Fe_{0.28}TaS_2$ is similar, but of opposite sign, to the magnetisation isotherms and both show broad hysteris loops (see figure 11).

The total Hall resistivity in ferromagnetic metals can be described by the empirical formula

$$\rho_{yx} = E_y/j_x = R_O B_z + \mu_0 R_S M_z \tag{2}$$

where E_y is the Hall field, j_x is the current density, $B_z = \mu_0[H_A + (1 - N_D)M_z]$ the z component of the internal magnetic induction, H_A the applied magnetic field along the z direction, N_D the demagnetising factor, R_O the ordinary Hall coefficient, R_S the spontaneous Hall coefficient, M_z the magnetisation in the direction of the applied field and μ_0 the permeability of vacuum. The first term describes the normal Hall effect due to the Lorentz force acting on the charge carriers. The carrier concentration can be deduced from the well known formula $R_O = (ne)^{-1}$, where n is the electron concentration

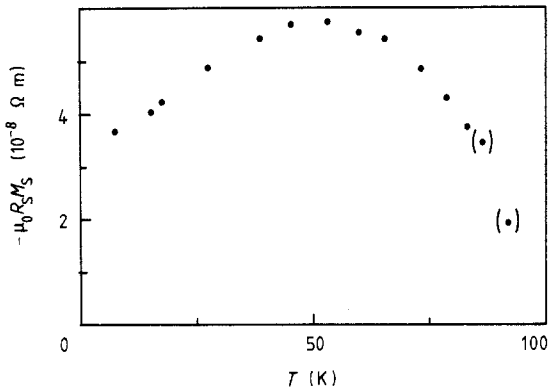

Figure 12. The temperature dependence of the spontaneous part of the Hall effect $\rho_S = \mu_0 R_S M_S$ of $Fe_{0.28}TaS_2$.

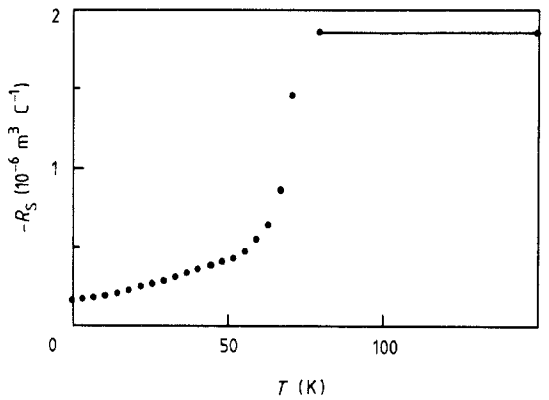

Figure 13. The temperature dependence of the spontaneous Hall coefficient R_S of $Fe_{0.28}TaS_2$.

and $-e$ the electron charge. When holes are the predominant current carriers, R_O is positive.

The second term of equation (2) is only present in materials with a spontaneous magnetisation and is associated with the asymmetric scattering of the conduction electrons at the local magnetic moments (Hurd 1972). Generally R_S is much larger than R_O. In this section R_O and R_S will be calculated from the Hall resistivity measurements.

Because the Hall measurements were performed on thin plates with $N_D = 1$, equation (2) reduces to

$$\rho_{yx} = R_O \mu_0 H_A + R_S \mu_0 M_z.$$

Hall resistivity ρ_{yx} isotherms as a function of the applied field were measured using a five-point method.

Below T_C the spontaneous contribution $\rho_S = R_S \mu_0 M_S$ (figure 12) to ρ_{yx} can be obtained by the extrapolation of the saturation part of ρ_{yx} to zero magnetic induction, which corresponds to zero applied field H_A, since $N_D = 1$. The spontaneous Hall coefficient R_S (figure 13) can be calculated by dividing ρ_S by the measured value of $\mu_0 M_S$ (figure 7) at the same temperature.

The spontaneous Hall coefficient R_S increases with temperature. For an ideal crystal with perfect magnetic ordering R_S should be zero at 0 K, but in our non-stoichiometric sample there is already some (asymmetric) scattering at low temperatures, resulting in a value R_S (0 K) $= -2.0 \times 10^{-7}$ m^3 C^{-1}.

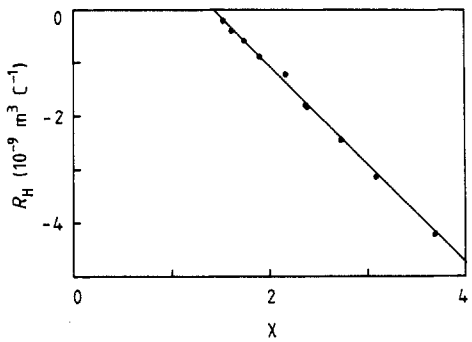

Figure 14. The slope of the Hall coefficient R_H versus the magnetic susceptibility χ at temperatures above the Curie temperature.

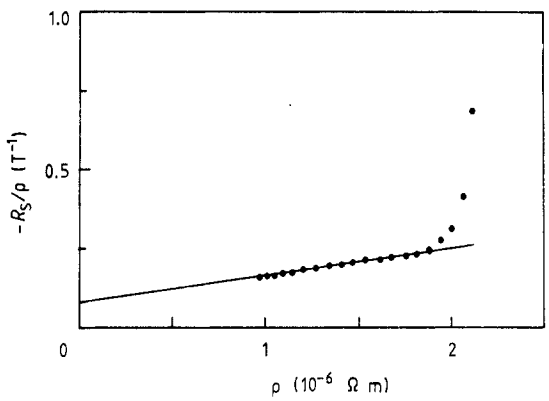

Figure 15. The R_S/ρ versus ρ plot for determination of the skew scattering and the side jump contribution to the spontaneous Hall coefficient. The linear fit is shown by the straight line.

Below T_C the slope of ρ_{yx} versus the applied field in the saturation region is $\partial\rho_{yx}/\partial(\mu_0 H_A) = R_O + \chi_i R_S$, where χ_i is the internal magnetic susceptibility above technical saturation ($\chi_i = \partial M_z/\partial H_A$). At temperatures well below T_C, say below $0.5T_C$, χ_i is so small that the second term can be neglected and R_O can be obtained. The slope of ρ_{yx} versus H_A at 4.2 K gives $R_O = +2.7 \times 10^{-9}$ m^3 C^{-1}. This corresponds to a hole concentration $p = (eR_O)^{-1} = 0.14$ holes per Ta atom.

At temperatures above T_C the magnetisation can be described with the paramagnetic susceptibility χ, and the Hall resistivity is given by $\rho_{yx} = (R_O + \chi R_S)\mu_0 H_A$. When the Hall coefficient $R_H = \rho_{yx}/\mu_0 H_A$ is plotted as a function of χ, a straight line results (figure 14). With the assumption that R_O and R_S are temperature-independent above T_C, R_O can be calculated from the intercept with the vertical axis and R_S from the slope of the line. In this way we find $R_O = +2.66 \times 10^{-9}$ m^3 C^{-1} and $R_S = -1.86 \times 10^{-6}$ m^3 C^{-1} in the paramagnetic region. R_S is orders of magnitude larger than R_O and of opposite sign.

The R_O values at 4.2 K and above T_C are the same, indicating a temperature-independent carrier concentration of 0.14 holes per Ta. The agreement with the result of our band-structure calculation is good—both give 0.14 hole per Ta—but not as satisfactory as it seems: the calculation is for $x_{Fe} = 1/3$, while the experimental value was measured on a sample with $x_{Fe} = 0.28$.

4.4. Discussion

All experimental data for $Fe_{1/3}TaS_2$ presented above support the results of the ASW band-structure calculations. Magnetic measurements (magnetisation, susceptibility and coercive forces) show Fe in $Fe_{0.28}TaS_2$ to be close to the high-spin Fe^{2+} state. A metallic resistivity is measured and from the temperature-independent ordinary Hall coefficient R_O a hole concentration in the Ta $5d_{z^2}$ band is calculated, which is smaller than one would expect when Fe is divalent. Thus Fe in $Fe_{1/3}TaS_2$ is more ionised than 2+, a conclusion supported by Mössbauer measurements (Eibschütz *et al* 1975, 1981).

The magnetic measurements on $Fe_{0.28}TaS_2$ below and above T_C (saturation moment 3.86 μ_B and $\mu_{eff} = 3.85\ \mu_B$) show that the best way to describe the Fe ions is as high-spin Fe^{2+}. A quantitative comparison with the band-structure calculation is hampered by the non-stoichiometry of the sample.

Defining q_c as the number of Bohr magnetons deduced from the Curie–Weiss constant by $\mu_{eff} = [q_c(q_c + 2)]^{1/2}\ \mu_B$, the observed value $\mu_{eff} = 3.85\ \mu_B$ gives $q_c = 2.98$. The saturation moment is $q_s = 3.86\ \mu_B$. In local moment ferromagnets $q_c/q_s = 1$, and in itinerant ferromagnets this ratio is larger than one (Rhodes and Wohlfahrt 1963, Wohlfahrt 1978). For $Fe_{0.28}TaS_2$ we find $q_c/q_s = 0.77$. A ratio q_c/q_s less than one was also found in the Heusler alloys CoMnSb, NiMnSb and PtMnSb (Otto *et al* 1989a), where it was attributed to the magnetic depolarisation at higher temperatures of the conduction band, which carries at low temperatures a non-negligible part of the magnetisation. A similar effect can be present in $Fe_{1/3}TaS_2$, where according to the band-structure calculations also a substantial part of the magnetisation is carried by the Ta $5d_{z^2}$ conduction electrons.

The anomalous Hall effect is caused by asymmetric scattering of the charge carriers, with two contributions: skew scattering and side jump (Smit 1958, Berger 1970, Berger and Bergmann 1980, Nozieres and Lewiner 1973, Asomoza *et al* 1983). A simple phenomenological description was given by Otto *et al* (1989b). For a ferromagnetic metal with local magnetic moments and magnetically polarised charge carriers, the anomalous Hall effect can be written as a function of the total resistivity ρ:

$$R_S = a\rho + b\rho^2 \tag{3}$$

with $a = \alpha \tan \phi$ and $b = \alpha p e^2 \Delta y / m^* v_F$, $\alpha = (\Delta p/p)\mu_0 M_S$ and $\Delta p = (p_\uparrow - p_\downarrow)$. The coefficient α describes the relative spin polarisation of the conduction electrons. The skew scattering angle is ϕ, the side jump Δy, and p is the concentration of the holes with effective mass m^* and velocity v_F. In order to analyse the anomalous Hall effect of $Fe_{0.28}TaS_2$ in terms of skew scattering and side jump, a plot is made of R_S/ρ versus ρ (figure 15). Up to 0.8 T_C a linear relation is observed. The intercept with the vertical axis and the slope give the coefficients $a = -0.082\ T^{-1}$ and $b = -8.6 \times 10^4\ T^{-1}\ \Omega^{-1}\ m^{-1}$.

For the calculation of the skew scattering angle ϕ and the side jump Δy of $Fe_{0.28}TaS_2$ we have to estimate values for α (or $\Delta p/p$), n, v_F and m^*. In view of the crudeness of the model we will not try to do better than the free-electron approximation for m^* and v_F. The charge carrier concentration obtained from the normal Hall effect is $p = 2.34 \times 10^{27}\ m^{-3}$. With the value $\Delta p/p = 0.43$ from our band-structure calculations, we find for the skew scattering angle a value $\phi = -2.28°$ and side jump $\Delta y = -3.8 \times 10^{-10}$ m.

In order to compare the data for $Fe_{0.28}TaS_2$ with the results for other compounds it is useful to define a parameter $B = \Delta y / m^* v_F$, which is independent of the total

magnetisation and the number of charge carriers; it describes a property per conduction electron or hole. For $Fe_{0.28}TaS_2$ we find $B = -7 \times 10^{-4}$ s kg^{-1}.

Otto *et al* (1989b) found in the Heusler alloys values for ϕ between $-0.76°$ and $+1.2°$ and for B between 0.8×10^{13} and 5.1×10^{13} s kg^{-1}. For US and USe skew scattering angles of $-0.97°$ and $-1.83°$, respectively, and a side jump parameter $B = +10.2 \times 10^{13}$ s kg^{-1} for both compounds are found, assuming complete spin polarisation of the conduction electrons (Feil 1987). The skew scattering angle ϕ and especially the side jump parameter B of $Fe_{0.28}TaS_2$ are very large, probably due to the contributions of orbital momentum of the Fe atoms to the asymmetric scattering.

5. Conclusions

ASW band-structure calculations of the ferromagnetic metallic compounds $Fe_{1/3}TaS_2$ and $Mn_{1/3}TaS_2$ show that the electronic structure of these intercalates can be understood only in first approximation in terms of the rigid-band model. It is found indeed that the TaS_2 part of the band structure is roughly the same as in the host 2H-TaS_2, but with some electrons transferred from the intercalant 3d atoms to the Ta $5d_{z^2}$ band. However, band-structure calculations can give more detailed information about the intercalant 3d states. It is found that Mn is divalent, leaving 0.30 holes per Ta in the Ta $5d_{z^2}$ band. The Fe valency lies in between 2+ and 3+, leaving 0.14 holes in the Ta $5d_{z^2}$ band. The calculated 3d bands are narrow and show the expected octahedral crystal-field splitting. The local magnetic moments on the intercalant sites are 4.4 μ_B for Mn and 3.6 μ_B for Fe. Through covalency also the Ta $5d_{z^2}$ conduction band becomes magnetically polarised. This effect is stronger in the case of Mn, where this polarisation amounts to 73%, than for Fe (43%). The polarisation of the conduction band is antiparallel to that of the intercalant moments in $Mn_{1/3}TaS_2$, while it is parallel in $Fe_{1/3}TaS_2$. Another striking deviation from the rigid-band model is the increase of the Ta 5d/S 3p gap by about 1 eV, due to the increase in ionicity in the Ta–S bond.

Magnetic and transport measurements on $Fe_{0.28}TaS_2$ support the calculated electronic structure. A saturation magnetisation at 4.2 K of 3.86 μ_B per Fe is measured, while above the Curie temperature ($T_C = 70$ K) a Curie–Weiss fit of the susceptibility gives $\mu_{eff} = 3.85\ \mu_B$. At low temperatures large coercive fields are observed.

From the normal Hall coefficient R_O a hole concentration of 0.14 holes per Ta is calculated, in agreement with the ASW band structure.

The electrical resistivity shows a strong interaction between the Ta $5d_{z^2}$ conduction electrons and the local magnetic moments. This interaction is also responsible for the large anomalous Hall effect, which is analysed in terms of skew scattering and side jump contributions. The side jump is very large compared with values measured for other compounds.

Acknowledgments

We thank H H Weitering for the $Fe_{0.28}TaS_2$ samples. One of us (RA de G) wants to thank the Stichting voor Fundamenteel Onderzoek der Materie (FOM) for financial support.

References

Asomoza R, Fert A and Reich R 1983 *J. Less Common Met.* **90** 177

Barry J J and Hughes H P 1982 *J. Phys. C: Solid State Phys.* **15** L797

—— 1983a *J. Phys. C: Solid State Phys.* **16** 5393

—— 1983b *J. Phys. C: Solid State Phys.* **16** L275

Beal A R 1979 *Physics and Chemistry of Materials with Layered Structures* vol. 6 *Intercalated Layer Materials* ed. F A Levy (Dordrecht: Reidel) p 251

Berger L 1970 *Phys. Rev.* B **2** 4559

Berger L and Bergmann G 1980 *The Hall Effect and its Applications* ed. C L Chien and C R Westgate (New York: Plenum) p 55

Coqblin B 1977 *The Electronic Structure of Rare-Earth Metals and Alloys: The Magnetic Heavy Rare Earths* (New York: Academic)

Dijkstra J, Broekhuizen E A, van Bruggen C F, Haas C, de Groot R A, van der Meulen H P 1989 to be published

Eibschütz M, di Salvo F J, Hull G W and Mahajan S 1975 *Appl. Phys. Lett.* **27** 464

Eibschütz M, Mahajan S, di Salvo F J, Hull G W and Waszcak J V 1981 *J. Appl. Phys.* **52** 2098

Feil H 1987 *Thesis* Groningen

Friend R H and Yoffe A D 1987 *Adv. Phys.* **36** 1

Guo G Y and Liang W Y 1987 *J. Phys. C: Solid State Phys.* **20** 4315

Hedin L and Lundquist B I 1971 *J. Phys. C: Solid State Phys.* **4** 2064

Hulliger F and Pobitschka E 1970 *J. Solid State Chem.* **1** 117

Hurd C M 1972 *The Hall Effect and its Applications* (New York: Plenum)

International Tables for Crystallography 1983 vol A (Dordrecht: Reidel) p 566

Methfessel M and Kübler J 1982 *J. Phys. F: Met. Phys.* **12** 141

Nozieres P and Lewiner C 1973 *J. Physique* **34** 901

Otto M J, van Woerden R A M, van der Valk P J, Wijngaard J, van Bruggen C F and Haas C 1989b *J. Phys.: Condens. Matter* **1** 2351

Otto M J, van Woerden R A M, van der Valk P J, Wijngaard J, van Bruggen C F, Haas C and Buschow K H J 1989a *J. Phys.: Condens. Matter* **1** 2341

Parkin S S P and Beal A R 1980 *Phil. Mag.* **42** 627

Parkin S S P and Friend R H 1980a *Phil. Mag.* **41** 65

—— 1980b *Phil. Mag.* **41** 95

Parkin S S P, Marseglia E A and Brown P J 1983 *J. Phys. C: Solid State Phys.* **16** 2749

Rhodes P and Wohlfahrt E P 1963 *Proc. R. Soc.* A **273** 247

Smit J 1958 *Physica* **24** 39

Suzuki N, Yamasaki T and Motizuki K 1987 *J. Magn. Magn. Mater.* **70** 64

Van den Berg J M and Cossee P 1968 *Inorg. Chim. Acta* **2** 143

Van den Berg-Voorhoeve J M 1976 *Physics and Chemistry of Materials with Layered Structures* vol 4 *Optical and Electrical Properties* ed. P A Lee (Dordrecht: Reidel) p 423

Van Laar B, Rietveld H M and Ijdo D J W 1970 *J. Solid State Chem.* **3** 154

Wijngaard J W, Dijkstra J, de Groot R A, Feil H and Haas C 1988 *J. Physique Coll.* **C8** 1505

Williams A R, Kübler J and Gelatt C D Jr 1979 *Phys. Rev.* B **19** 6094

Wohlfahrt E P 1978 *J. Magn. Magn. Mater.* **7** 113